Carbon 249 (2026) 121244

Contents lists available at ScienceDirect

Carbon

journal homepage: www.elsevier.com/locate/carbon

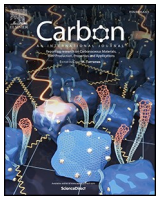

The effect of carbon support on rhenium-catalyzed glyceric acid deoxydehydration into biobased acrylic acid

Maja Gabrič [a,d], Brigita Hočevar [a], Anej Blažič [a,d], Janvit Teržan [a,c], Sašo Gyergyek [b], Blaž Likozar [a], Miha Grilc [a,d,*]

[a] Department of Catalysis and Chemical Reaction Engineering, National Institute of Chemistry, Hajdrihova 19, 1000, Ljubljana, Slovenia
[b] Department for Materials Synthesis, Jožef Stefan Institute, Jamova 39, Ljubljana, 1000, Slovenia
[c] Center for Development, Demonstration and Training for Carbon-Free Technologies, National Institute of Chemistry, Hajdrihova 19, 1000, Ljubljana, Slovenia
[d] University of Nova Gorica, Vipavska Cesta 13, 5000, Nova Gorica, Slovenia

ARTICLE INFO

Keywords:
Carbon support
Bio-based acrylic acid
Glyceric acid
Deoxydehydration
Rhenium oxides catalysts

ABSTRACT

The influence of carbon support structure on the dispersion, oxidation state, and catalytic activity of rhenium species was systematically investigated in the deoxydehydration (DODH) of bio-based glyceric acid towards acrylic acid. Rhenium-based catalysts (targeting 5 wt% Re) were prepared by incipient wetness impregnation on activated carbons, carbon black, graphite, glassy carbon, and multiwalled carbon nanotubes. Comprehensive characterization by N_2 physisorption, scanning transmission electron microscopy, X-ray fluorescence, CO pulse adsorption, and X-ray photoelectron spectroscopy revealed that the support choice strongly affected rhenium particle size distribution, accessibility, and stabilization of oxidation states. Catalytic tests conducted at 150 °C under inert atmosphere in methanol solvent, identified activated carbon supports as the most effective, reaching combined selectivities up to 83 % toward DODH products (acrylic acid and methyl acrylate), comparable to those of the commercial Re/C catalyst. In contrast, the carbon black – supported catalyst exhibited very low activity toward DODH products, while the other carbon materials were practically inactive. The superior performance of activated carbon supports is due to the high surface area and mesoporous structure, which promotes better dispersion and accessibility of the active high valent Re species. These results highlight the decisive role of carbon support morphology and surface chemistry in governing the performance of rhenium catalysts, providing guidelines for the rational design of carbon-supported systems for biomass valorization.

1. Introduction

To reduce dependency on fossil fuels and petrochemical processing for polymer industry, the utilization of renewable alternatives such as biomass has gained increase attention. Biomass derived feedstocks present a sustainable and more environmentally friendly alternatives for producing acrylic acid (AA) and acrylate esters, which are widely used in coatings, adhesives, and absorbents [1–3]. One of the promising bio-based precursors to acrylic acid is also glycerol, a main byproduct of bio-diesel production [4,5]. The valorization of bioglycerol into acrylic acid depends on reducing its oxygen content through several reaction pathways [3,6,7], among which the deoxydehydration (DODH) reaction represent direct conversion of polyols to alkenes [8–11]. For DODH reaction, rhenium (Re) catalyst have shown significant potential [12]. Both homogeneous [13–16] and heterogeneous rhenium-based catalyst have been investigated. Among heterogeneous catalysts different oxide supports [17–19], particularly CeO_2 [20–24], and carbon-based materials [25–30], have been intensively studied.

Carbon materials have been widely applied as versatile catalyst support for many reactions and applications, owing to their good thermal stability, chemical resistance to acidic and basic conditions, adjustable hydrophobicity and polarity, and cost-effectiveness relative to many conventional supports [31–33]. The catalytic properties of carbon-supported catalysts vary with the underlying carbon structure [34–36]. The main categories of carbon-based catalysts include graphene [37,38], graphitic carbon nitride [39], carbon nanotubes [40–42] and activated carbon [18,25,43–51]. These latter materials provide high surface area and porosity, with surface-active sites arising from diverse functional groups—such as carboxyl, phenol, lactone, ether, and nitrogen-containing groups [52–54].

* Corresponding author. Department of Catalysis and Chemical Reaction Engineering, National Institute of Chemistry, Hajdrihova 19, 1000, Ljubljana, Slovenia.
E-mail address: miha.grilc@ki.si (M. Grilc).

https://doi.org/10.1016/j.carbon.2026.121244
Received 29 October 2025; Received in revised form 22 December 2025; Accepted 5 January 2026
Available online 8 January 2026

Carbon-based materials serve as supports for a wide range of metals, including rhenium. Various studies have been made on rhenium on carbon support for different reaction of hydrodeoxygenation [44,55,56], hydrogenation [57,58] and deoxydehydration [25–27,30,59,60]. However, most of these focus on the effect of reaction condition, such as temperature and reactant composition, rather than the effect of the catalyst structures. Blanco et al. observed how different surface functional groups on carbon supports can significantly influence the alloying state of metallic rhenium [48–50]. The carbon materials commonly investigated in these studies are mostly activated carbon and carbon nanotubes.

In our previous work of DODH conversion of mucic acid to adipic acid [26,27,30] and glyceric acid to acrylic acid [25,59] the commercial rhenium on carbon support showed exceptional activity. Therefore, this study was conducted to find out whether the catalytic activity of rhenium supported on various carbon materials for the DODH of glyceric acid is comparable to that of the commercial Re/C catalyst. The synthesized catalysts were tested under the optimal conditions identified in our previous study on commercial Re/C, namely at 120 and 150 °C in methanol, used as both solvent and hydrogen donor. The morphology and surface chemistry of carbon supports influence the dispersion and chemical state of rhenium species [49,61,62], therefore different types of activated carbon materials, carbon nanotubes and graphite carbon were tested as supports for the DODH reaction with rhenium. Demonstrating that the synthesized rhenium-on-carbon catalysts can achieve performance comparable to, or exceeding, that of commercial counterparts would offer a cost-effective and customisable alternative, enabling the rational design of catalysts for industrial-scale applications. Although the present study employs commercially available carbon supports, the same preparation method can readily be applied to bio-based carbons. Using renewable supports would reduce dependence on fossil-derived materials and align with circular-economy principles, thereby improving the overall sustainability of the catalytic process. In the long term, integrating bio-based carbon supports with efficient rhenium-based DODH catalysts could enable a fully bio-derived route to acrylic acid production, combining environmental benefits with economic viability.

2. Experimental

2.1. Synthesis of catalysts

The catalytic materials were prepared by incipient wetness impregnation (IWI) with an aqueous solution of ammonium perrhenate (NH_4ReO_4; Sigma Aldrich, Germany). The metal loading was calculated as 5 wt% Re on carbon. A range of commercial carbon-based supports with different structural and physicochemical properties were used in this study. The supports and the corresponding abbreviations referred to in this article are summarised in Table 1.

Before impregnation, the carbon support was crushed with a mortar and pestle, and sieved to obtain a homogeneous sample, which was then dried at 110 °C for 2 h. The calculated amount of NH_4ReO_4 (0.072 g of NH_4ReO_4 for 1g of catalyst) was dissolved in a 10 ml of deionised water and added directly onto the carbon material in a mortar while thoroughly mixing to ensure uniform distribution. After impregnation with the ammonium perrhenate, the catalysts were dried in an oven at 110 °C overnight. Immediately after drying, the catalysts were reduced in a tube furnace for 3 h at 400 °C (5 °C min^{-1}) in a hydrogen stream (0.2 L_N min^{-1}).

2.2. Catalyst characterisation

All catalyst were characterized by the following techniques.

To obtain adsorption and desorption isotherms the N_2 physisorption experiments at −196 °C were performed for all fresh catalyst. From those, the respective specific surface area (using the BET model), pore volume and average pore width ware determined. The measurements were performed on a Micromeritics ASAP 2020 analyser (Micromeritics Instrument Corporation, USA), degassing at 200 °C to 3 μm Hg for 17 h with 70 mg of the sample. Size of rhenium species and their distribution on carbon supports was observed by Thermo Fisher Scientifiry Talos F200i (USA) scanning transmission electron microscope (STEM) operated at 200 kV. High-angle annular dark-field (HAADF) and bright-field (BF) detectors were used simultaneously. Elemental maps were acquired using Energy dispersive X-ray spectroscopy EDXS in STEM mode. The dry samples were dispersed in isopropanol, deposited on a carbon-coated Cu specimen grid and left to dry naturally. Energy-dispersive X-ray fluorescence (XRF) spectroscopy was used to quantify elemental composition of the samples. Measurements were conducted with a Thermo Scientific™ ARL™ QUANT'X EDXRF Spectrometer, equipped with an SDD500 silicon drift detector. Samples were mounted in dedicated sample holders and analysed under vacuum conditions to enhance the detection of light elements. For the detection of rhenium, the measurement was performed using a Pd Medium filter at 20 kV and 2 mA tube current, under atmospheric pressure, with a total acquisition time of 30 s. A calibration curve was made using ammonium perrhenate (NH_4ReO_4; Sigma-Aldrich, Germany) as the standard, deposited at varying concentrations onto carbon support (Riogen Inc., USA). Data were processed using the instrument's proprietary software, utilizing both fundamental parameter models and external calibration where applicable. Carbon monoxide pulse adsorption (CO-PA) measurements were performed on both fresh and spent catalysts using a Microtrac BELCAT II chemisorption analyser coupled to a BELMASS II-62 quadrupole mass spectrometer (Microtrac, Haan, North Rhine-Westphalia, Germany). Prior to analysis, the catalysts were pre-treated in a 5 vol% H_2/Ar gas mixture (30 ml min^{-1}) at 400 °C (4 °C min^{-1}) for 180 min. After pre-treatment, the samples were exposed to ten pulses of 5 vol% CO in He. Each CO pulse was monitored using the CO fragment (m/z = 28), and the area under each peak was integrated. The last 3 pulses, exhibiting the constant areas, were used to calibrate the signal to the number of moles of CO injected. The chemisorbed CO for each earlier pulse was calculated by comparing its area to the saturated average. The total CO uptake was obtained by summing the CO consumption over all unsaturated pulses. The dispersion (D) of the Re was calculated by dividing the Re surface metal atoms to the total number of Re atoms

Table 1
Listed carbon-based supports with supplier and origin information.

Abbreviation of catalyst	Support Name	Description	Supplier
ReO_x/AC1	High Surface Area Carbon Support	>98 %;	Riogen Inc., USA
ReO_x/AC2	Activated Charcoal DARCO	100 mesh particle size, powder;	Sigma Aldrich, Germany
ReO_x/AC3	Mesoporous Carbon	surface area: >500 m^2 g^{-1}, BET; pore size: 0.4–0.7 cm^3 g^{-1} mesoporosity 0–0.25 cm^3 g^{-1} microporosity	Sigma Aldrich, Germany
ReO_x/CB	Carbon Black Vulcan XC 72	325 mesh residues, powder;	Cabot Corporations, USA
ReO_x/GC	Glassy Carbon	Glassy, spherical powder, 2–12 μm, 99.95 % trace metals basis;	Sigma Aldrich, Germany
ReO_x/GP	Graphite Powder	200 mesh, 99.9 %;	Thermo Scientific Chemicals, USA
ReO_x/MWCNT	Multi-Walled Carbon Nanotubes	>99 %;	NTL Composites, India

present in the catalyst. The oxidation states of rhenium were determined by X-ray photoelectron spectroscopy (XPS) with the PHI VersaProbe 3 AD (Phi, Chanhassen, USA), which uses a monochromatic Al Kα X-ray source. For charge neutralisation, the charge of the sample was attenuated with two beams (electrons and ions). The peak shift caused by the neutralisation was corrected by shifting the peaks of the random carbon species to 284.8 eV. The spectra were measured at a transit energy of 224 eV with a step size of 0.8 eV. The high-resolution spectra were measured with a transit energy of 50 eV and a step size of 0.05 eV. Two sweeps were performed for the survey spectra, while 10 sweeps were performed for the high-resolution spectra. The spectral deconvolution was performed with the Khervefitting software.

2.3. Catalytic activity

Catalytic deoxydehydration experiments were performed in high-pressure, high-temperature autoclave batch reactors (Parr 5000 Multi Reactor System, 75 mL total volume per reactor). Each reactor was independently heated (controlled by a thermocouple inside the reactor vessel) and stirred via magnetic stirrers and was equipped with pressure gauges, gas inlet (N_2, 5.0, Messer, Germany) and outlet valves and a liquid sampling line. In a typical catalytic experiment, 500 mg of aqueous glyceric acid (GA; LD-2,3-dihydroxypropanoic acid; 20–22 wt% in water, TCI Chemicals, Japan) and 45.0 mL of methanol (MeOH; >99.8 %, J.T. Baker, USA) were weighed and added to the autoclave reactor vessel to obtain a 20 mM reactant solution. The catalyst was added to this solution, e.g. 140 mg of pre-reduced selected catalyst. The reactor was closed, sealed and purged three times with N_2 gas before setting a N_2 pressure of 5 bar_g. The stirring speed was set to 800 min^{-1}. The reactor was heated to the final reaction temperature (usually 150 °C) within about 30 min and kept at that temperature for 72 h. The reactor was then cooled down to room temperature, depressurized, purged with N_2 and opened to collect the product mixture. This liquid product mixture and the liquid samples taken during the reaction were filtered and analysed by gas chromatography (GC) and high-pressure liquid chromatography (HPLC). GC was used to determine the presence of methyl acrylate (MA), methyl glycerate and methyl propanoate, while HPLC analysis was used to determine the concentrations of glyceric acid and acrylic acid. Propanoic acid could not be detected under the HPLC conditions used, and therefore no results are reported for this compound. With GCMS it was possible to quantify propanoic acid, however due to overlapping with acrylic acid, quantification was not possible. For GC analysis a Shimadzu GCMS-QP 2010 Ultra (Japan) gas chromatograph equipped with a Zebron ZB-5MS capillary column (60 m × 0.25 mm x 0.25 μm), a flame ionization detector (FID) and a quadrupole mass spectrometry (MS) was used. The Thermo-Fisher Scientific UltiMateTM 3000 UHPLC with DAD and RI was used to determine the amount of acrylic acid and glyceric acid. The column used was the Supelcogel 8 % (9 μm particle size, L × I.D. 30 cm × 7.8 mm) (Sigma Aldrich, Germany), with a guard column of the same type. The mobile phase was 5 mM H_2SO_4 (18.2 MΩ). The column was kept at 40 °C with a flow rate of 0.6 mL min^{-1}. Detection was performed with the UV detector at a wavelength of 205 nm. After quantification of the products using 5-point calibration curve, the conversion (C [%]) and selectivity (S [%]) were calculated using the following equations:

$$C\,[\%] = \frac{c^0_{GA} - c_{GA}(t)}{c^0_{GA}} \times 100$$

$$S\,[\%] = \frac{c_{product\ i}}{\sum c_{products}} \times 100$$

In this equation c^0_{GA} is the initial amount of glyceric acid (t_0), $c_{GA}(t)$ is the molarity of the glyceric acid at a time t, $c_{product\ i}$ is the amount (mol L^{-1}) of the product i. The carbon balances, based on the quantified components during the experiments, consistently exceeded 75 %.

To assess the stability of the catalyst and extent of rhenium leaching into the liquid phase, the reactor was first cooled to room temperature after the catalytic reaction. The solid catalyst particles were separated from the reaction mixture by filtration through polytetrafluoroethylene polymer (PTFE) filters (0.2 μm). The collected liquid was then analysed using XRF spectroscopy to quantify the total concentration of dissolved rhenium.

3. Results and discussion

3.1. Catalyst characterization

The textural properties of the bare untreated supports and the synthesized Re-based catalysts after impregnation were determined using N_2 sorption isotherms. The corresponding surface areas, total pore volumes and average pore width are given in Table 2. Some clear differences can be observed among the supports, all activated carbon supports (ACX) exhibit very high surface area (above 550 $m^2\ g^{-1}$), CB and MWCNT have a moderate surface area (174 and 90 $m^2\ g^{-1}$, respectively) with a high pore volume and GC and GP have very low surface area (2 and 3 $m^2\ g^{-1}$, respectively) and pore volume, suggesting negligible porosity. The pore size distributions derived from BJH analysis are shown in Fig. S1. Activated carbon based catalysts (ReO_x/AC1-3) exhibit dominant mesopores centred at approximately 4–5 nm with contribution of pores below 2 nm. ReO_x/CB shows broader mesoporosity, without distinct maximum peak. In contrast, ReO_x/MWCNT displays a very broad pore size distribution extending up to 30 nm, characteristic of intertubular voids rather than intrinsic porosity. As shown in Table S1, the surface areas and pore volumes of the supports without Re were consistently higher than those of the corresponding catalysts. This trend is generally attributed to partial pore filling or pore blocking by Re species deposited during the incipient wetness step, and is consistent with previous studies on Re-based catalysts prepared by similar methods [48]. The significantly higher surface areas and pore volumes of activated carbon compared to other carbon supports arise from its intrinsic mesoporous structure, which is developed during the activation process [63].

The nitrogen adsorption–desorption isotherms are presented in Fig. S2. ReO_x/AC1, ReO_x/AC2, and ReO_x/AC3 exhibit hybrid Type IV isotherms, with a steep N_2 uptake at low relative pressure ($p/p_0 < 0.1$) followed by an H4-type hysteresis loop. This combination is characteristic of mesoporous carbons with slit-shaped pores. ReO_x/CB shows a Type IV isotherm with pronounced H3-type hysteresis at high relative pressures, confirming the presence of mesopores. ReO_x/MWCNT also presents a Type IV isotherm but with a smaller hysteresis loop, reflecting mesoporosity arising from the cylindrical channels of the nanotubes. In contrast, ReO_x/GC and ReO_x/GP show nearly flat isotherms with negligible adsorption over the entire range of relative pressures, consistent with their non-porous or very low-porosity nature [64].

To get a better insight into the size and dispersion of Re (species) over the carbon supports in the selected catalysts, the STEM analysis (of pre-reduced catalyst at 400 °C with H_2 for 3 h) was conducted. In all the cases size of Re species is below 1 nm. Because of low number of atoms that clusters contain and consequently low contrast they appear smeared with not well-defined edges. For this reason, their precise size

Table 2
Textural properties of the synthetised catalysts.

	S_{BET} [$m^2\ g^{-1}$]	Pore volume [$cm^3\ g^{-1}$]
ReO_x/AC1	761	0.38
ReO_x/AC2	828	0.51
ReO_x/AC3	550	0.11
ReO_x/CB	174	0.53
ReO_x/GC	2	0.002
ReO_x/GP	3	0.02
ReO_x/MWCNT	90	0.70

distribution cannot be reliably determined. Catalysts ReO_x/AC1 and ReO_x/AC2 share similar morphology (Fig. 1a–d). Small Re clusters are uniformly distributed over the shapeless carbon support particles. Closer inspection reveals that in the case of ReO_x/AC1 Re clusters are the smallest among catalysts with a narrow size distribution (Fig. 1b–S3 and Table 3) while in the case of ReO_x/AC2 those are significantly larger (Fig. 1d–S3 and Table 3) and their size distribution is pronouncedly skewed toward larger sizes (Fig. S3). In addition to Re clusters some well-defined roughly 20–50 nm sized Fe or Fe-carbide nanoparticles are clearly seen in ReO_x/AC2. Their elemental analysis showed only presence of Fe and C therefore eliminating presence of Fe-oxides. Since those are already present in AC2 sample and Fe or Fe carbides are known for not being active catalyst for DODH of glyceric acid [8] their exact identification was not conducted. Re distribution in the ReO_x/AC3 catalyst is rather different (Fig. 1e and f). Besides small Re clusters (only those were measured and reported in Table 3) that are nearly twice in diameter as Re clusters in ReO_x/AC1, large agglomerates of Re nanoparticles are also clearly visible (Fig. 1f). The Vulcan carbon (CB) is composed of nearly spherical 10–40 nm sized particles that form loose agglomerates. Re clusters are non-homogenously distributed over their surfaces (Fig. 1g and h). Average size of Re clusters is slightly smaller than in the case of ReO_x/AC3 however it is significantly broader (Table 3 and Fig. S7) spanning well over 1 nm. MWCNTs are several microns in length, 10–20 nm in diameter and regularly contain Fe or Fe-carbide nanoparticles. Those are most likely residue since Fe nanoparticles are used as catalysts for MWCNT production [65]. Re clusters are rather uniformly dispersed over the MWCNTs surface (Fig. 1j) and of narrow size distribution with an average value close to average size of Re clusters in ReO_x/AC3 and ReO_x/CB (Fig. S3 and Table 3). Glassy carbon is in the form of several microns sized spherical particles which are not transparent to electron beam and consequently Re clusters were not seen or detected by EDXS. Graphite powder is in the form of several micron sized agglomerates of thin graphite sheets decorated with agglomerates of ZrO_2 nanoparticles, which are not active on their own for DODH reaction (Fig. S4) [66]. Those are contamination due to processing of graphite powder by the supplier. In ReO_x/GP subnanometre-sized Re clusters are visible on thin edges of the graphite sheets (Fig. S5).

To determine whether the actual Re loading after the reduction on each catalyst matched the expected value of 5 wt%, the XRF analysis was performed. The quantified Re content (wt.%) of each supported catalyst, measured before and after reduction, is presented in Table S2. Minor discrepancies in Re content before and after reduction can be attributed mostly to sample inhomogeneity, as Re being present in the clusters on the supports (Fig. 1, Fig. S6). For clarity and consistency in the article, these post-reduction XRF values will be used in all subsequent discussions of Re loading. For activated carbon supports, the Re loadings after reduction are 4.09, 5.46, and 3.72 wt% for AC1, AC2, and AC3, respectively. For other carbon supports, the post-reduction loadings are 5.34, 4.99, 2.30, and 4.60 wt% for CB, GC, GP, and MWCNT, respectively. These values suggest that on all carbons, Re was successfully impregnated in the range of 2.30–5.46 wt%, but since this does not represent the actual Re species available on the surface, CO-PA measurements were performed to determine the metal dispersion, quantify the surface Re sites, and estimate the size of the Re nanoparticles on the different carbon supports (Table 3).

For the activated carbon-based catalysts (ReO_x/AC1, ReO_x/AC2, ReO_x/AC3), a clear linear trend can be observed between the CO uptake and the specific surface area. The highest CO uptake was achieved with ReO_x/AC1 and ReO_x/AC2, which also agrees with the STEM results, showing highly dispersed Re nanoparticles mostly below 1 nm. On the other hand, the CO uptake is slightly lower for ReO_x/AC3, which could be attributed to the agglomeration and formation of larger clusters observed with STEM. A relatively high CO uptake was observed for the ReO_x/CB catalyst, although it has a lower surface area compared to ACX activated carbons. This indicates that CB causes a stronger stabilization of the Re nanoparticles, which is also evidenced by a homogeneous

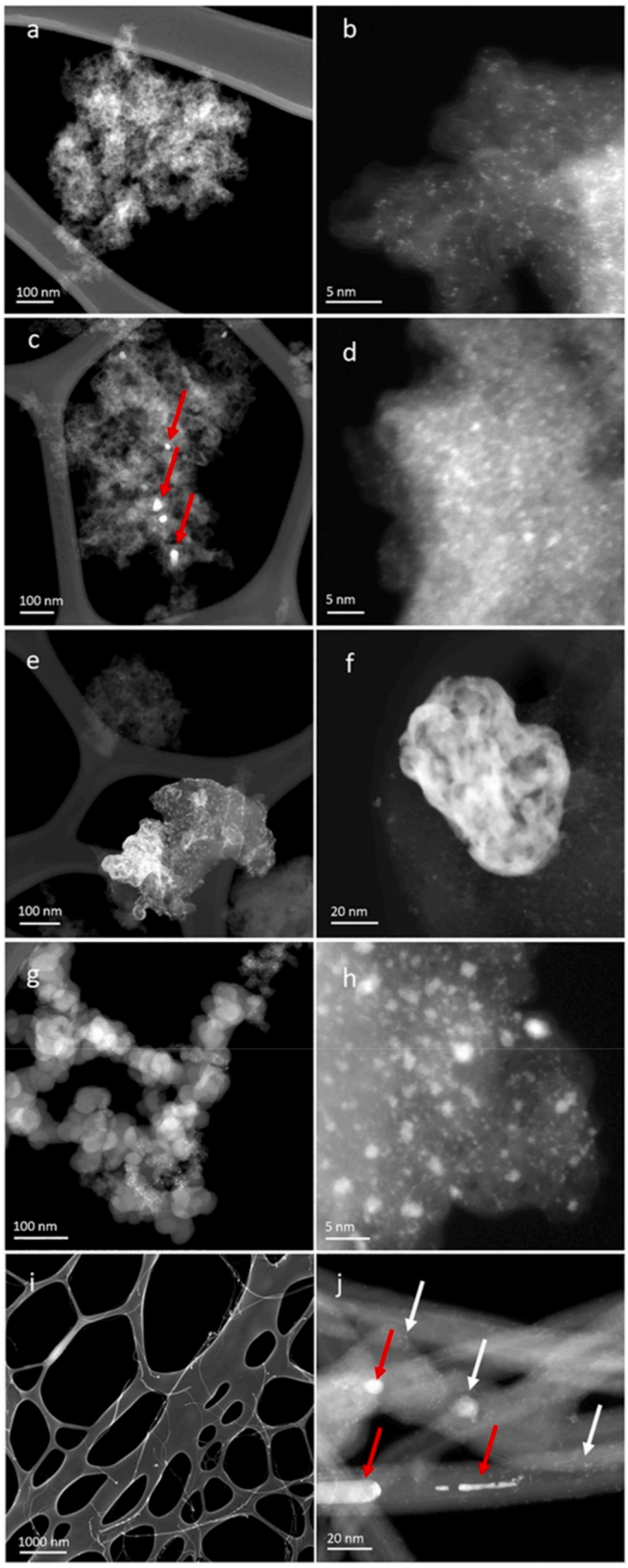

Fig. 1. Lower magnification and higher magnification HAADF-STEM images of the (a, b) ReO_x/AC1, (c, d) ReO_x/AC2, (e, f) ReO_x/AC3, (g, h) ReO_x/CB and (I, j) ReO_x/MWCNT. Red arrows point to Fe nanoparticles while white point to Re clusters.

Table 3
CO absorption and metal dispersion size of rhenium catalysts determined by CO-PA and rhenium clusters size determined from HAADF STEM images.

Catalyst	CO adsorption capacity [μmol g_{cat}^{-1}]	Dispersion [%]	d_{STEM} [nm]
ReO_x/AC1	12.0	4.5	0.27 ± 0.07
ReO_x/AC2	22.3	8.3	0.41 ± 0.23
ReO_x/AC3	7.1	2.6	0.68 ± 0.18
ReO_x/CB	8.2	3.1	0.61 ± 0.25
ReO_x/GC	<0.5	n.a.	n.a.
ReO_x/GP	<0.5	n.a.	n.a.
ReO_x/MWCNT	<0.5	n.a.	0.53 ± 0.05

*n.a.-not available; the catalyst were not able to be measured.

particle distribution and the absence of larger clusters in the STEM images. No CO uptake was observed on the catalysts ReO_x/GC, ReO_x/GP and, ReO_x/MWCNT indicating low metal availability on the surface, which is also consistent with the STEM analysis and SEM-EDX measurements. In Fig. S6 nonhomogeneous Re distribution and Re-rich aggregates on these supports can be seen.

X-ray photoelectron spectroscopy was used to determine how different carbon support stabilize various rhenium species. The Re4f region can be deconvoluted into several peaks, indicating a very complex oxidation profile of Re (Fig. 2). These results are consistent with earlier reports in the literature [67]. Interestingly, the oxidation profile is slightly different depending on the carbon. The highest amount of metallic Re was retained on the CB support, suggesting that the metallic Re nanoparticles are particularly stable on this support. In contrast, the activated carbon support facilitates the deep oxidation of Re, with the majority of Re in the 6+ oxidation state. The latter means that Re on such supports is very active for the activation of bonds. These results agree well with catalytic experiments in which the ReO_x/ACX materials clearly outperformed the other catalysts (vide infra).

It should be noted that the catalysts were exposed to air after the reductive pre-treatment during transfer to the spectrometer—similar to the exposure occurring during transfer to the reactor. Air exposure results in partial re-oxidation of Re, nonetheless, the objective of the study was to determine which support is more conducive to stabilizing various oxidation states of Re.

3.2. Catalytic tests

The catalyst support screening test for the DODH of glyceric acid was conducted at 150 °C for 72 h in inert atmosphere using seven different pre-reduced Re-based catalysts with various carbon supports (Table 1). To evaluate the potential catalytic activity of the blank reaction medium and AC1 carbon support itself, control experiments were performed. In both cases, no DODH products were detected (Fig. S7). The total selectivities are represented in Fig. 3 and Table S3 with corresponding conversions of DODH products reported after 24 h and 72 h. The reproducibility of the catalytic dehydroxylation of glyceric acid over ReO_x/AC1 in methanol solvent at 150 °C was assessed by conducting three independent experiments and calculating the corresponding

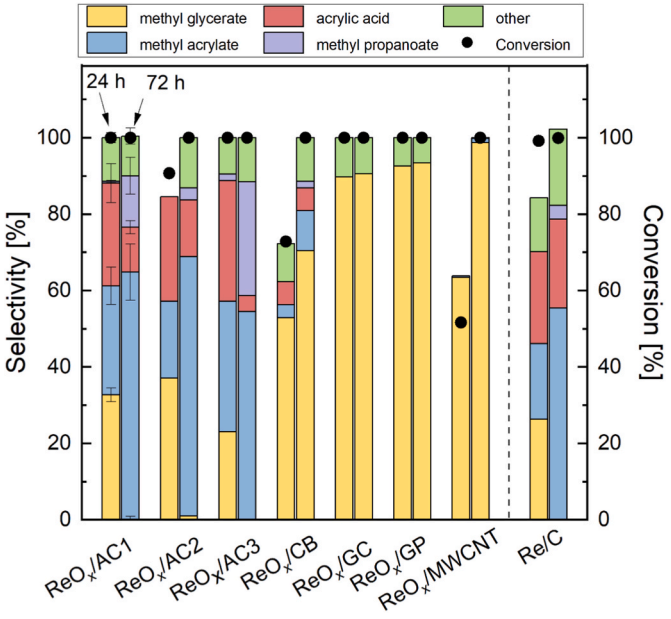

Fig. 3. Comparison of product selectivities in the DODH of glyceric acid over carbon supported Re catalyst after 24 and 72h at 150 °C under nitrogen atmosphere in methanol. The bars shown after the dashed vertical line correspond to the commercial 5 wt% Re/C catalyst, evaluated under identical reaction conditions.

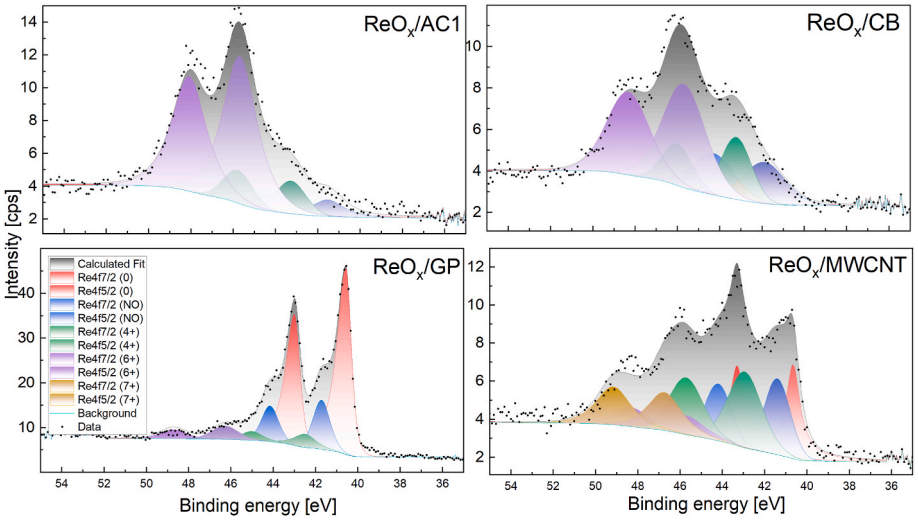

Fig. 2. XPS spectra of the Re 4 f region for the representative materials. All the measured catalysts were reduced prior to measurement. For both, the 4 f 7/2 peaks and the 4 f 5/2 peaks of Re (7+), Re (6+), Re(4+), Re(2+), and metallic Re are marked with brown, violet, green, blue and red, respectively. (For interpretation of the references to colour in this figure legend, the reader is referred to the Web version of this article.)

average product selectivities and standard deviations (Table S4). The results show decent reproducibility at all time points, with low standard deviations in product distributions.

Among the tested catalysts, the ones on activated carbon supports - ReO_x/AC1, ReO_x/AC2, and ReO_x/AC3- showed the highest selectivity toward the desired DODH products, AA and its ester MA, with combined selectivities after 72 h of 77 %, 83 %, and 59 %, respectively. These catalysts also displayed the highest turnover frequencies (TOFs) among the series, with values of 0.7, 0.4, and 1.1 h^{-1}, respectively (Table S5). These results indicate that the synthesized catalysts are comparably active to the commercially available Re/C catalyst [25]. After 24 h, the DODH is more selective towards acrylic acids which is subsequently esterified to methyl acrylate, consistent with the reaction mechanism presented in our previous study (Fig. 4) [25]. After 72 h, methyl acrylate can undergo further hydrogenation to form methyl propanoate, with corresponding selectivities of 13 %, 2 %, and 30 % for ReO_x/AC1, ReO_x/AC2, and ReO_x/AC3, respectively. This indicates that ReO_x/AC2 is the most selective toward primary DODH products, while ReO_x/AC3 tends to favour further hydrogenation. Activated carbon supports (AC1, AC2, AC3) have in common high surface areas and small pore volumes among the screened materials. This provides many accessible sites for rhenium anchoring and dispersion, a crucial factor for maximizing catalytic activity. For the successful DODH, Re nanoparticles must be well dispersed like on AC1 and AC2, where Re appears as highly dispersed, uniformly distributed nanoparticles or clusters, predominantly below 1 nm in size (Table S3).

Among the remaining supports, ReO_x/CB exhibited modest DODH activity, achieving a combined 9.4 % and 17 % selectivity for MA and AA, after 24 h and 72 h respectively. However, the dominant product in this case was methyl glycerate, suggesting limited DODH reactivity and a preference for esterification pathways, which can be correlated with lower availability of Re on the support (Table 3) due to its lower specific surface are (Table 2), and its non-homogenously distributed clusters on the support (Fig. 1). The other carbon-supported catalysts, ReO_x/GC, ReO_x/GP, and ReO_x/MWCNT, showed minor or no activity toward DODH products, with the product distributions dominated by methyl glycerate after 24 h and further than fully converts to it after 72 h. This indicates that Re is not available in the active form on these supports with poor textural and structural characteristics for dispersing or stabilizing Re species (Table 3). STEM and SEM analysis further confirms the absence and not uniformly observable Re particles (Fig. 1, S6) for ReO_x/GC, ReO_x/GP and ReO_x/MWCNT.

To further investigate the influence of reaction temperature on product distribution, selected pre-reduced catalysts—ReO_x/AC1 and ReO_x/AC3—were evaluated at 120 °C and 150 °C for 72 h under an inert N_2 atmosphere. The product selectivities and overall glyceric acid conversion are shown in Fig. 5 and Table S6. At the lower temperature the selectivity toward the targeted DODH products decreased significantly. Specifically, ReO_x/AC1 achieved a combined selectivity of 46.4 % for MA and AA, compared to 28.1 % for ReO_x/AC3. At 120 °C, methyl glycerate remained the dominant product—44.8 % for ReO_x/AC1 and

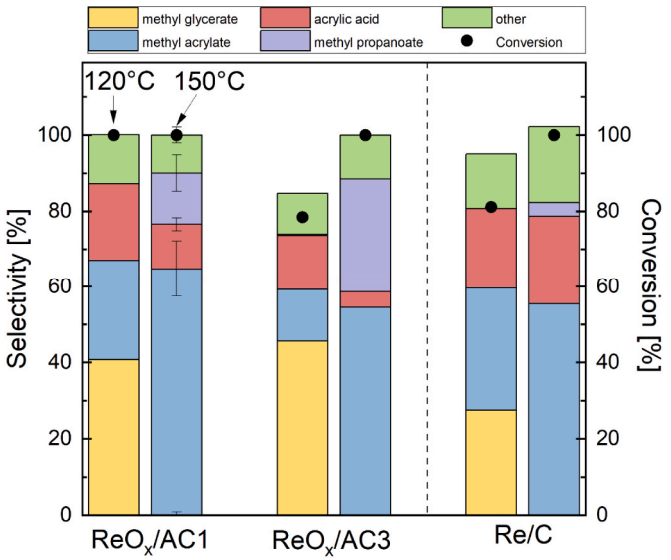

Fig. 5. Comparison of product selectivities at DODH for the selected carbon supported Re catalyst after 72h at 120 °C and 150 °C under nitrogen atmosphere in methanol. The bars shown after the dashed vertical line correspond to the commercial 5 wt% Re/C catalyst, evaluated under identical reaction conditions.

45.6 % for ReO_x/AC3—indicating incomplete conversion of the intermediate or a slower DODH step. However, the higher absolute yields of MA and AA on ReO_x/AC1 suggest more efficient DODH turnover on this catalyst even at lower temperature. These results align well with the proposed reaction mechanism previously observed for the commercial Re/C catalyst (Fig. 4) [25].

While one important role of the support is to ensure adequate dispersion of Re species for DODH of glyceric acid, another function is the stabilization of Re and its appropriate oxidation states. In the representative active catalyst ReO_x/AC1, based on an activated carbon support, Re is present in oxidation states ranging from +6 down to below

Table 4
Approximative surface concentration of rhenium oxidation states calculated from the area ratios from XPS on pre-treated Re supported catalyst used for glyceric acid conversion.

	Relative content [%]			
	ReO_x/AC1	ReO_x/CB	ReO_x/GP	ReO_x/MWCNT
Re (0)	0	0	67	24
Re (NO)	11	21	19	22
Re (4+)	15	26	6	28
Re (6+)	74	52	8	9
Re (7+)	0	0	0	17

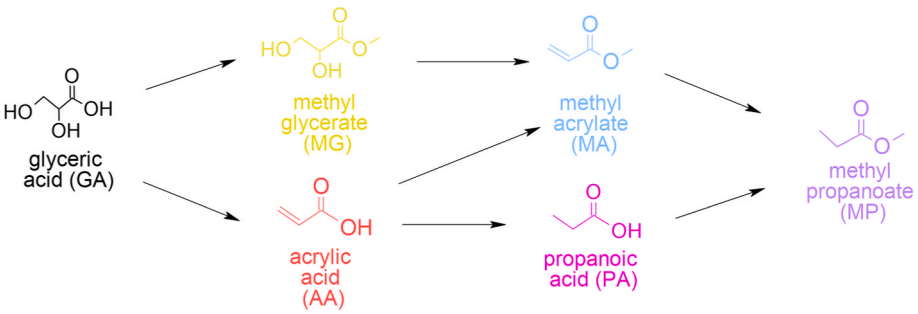

Fig. 4. Proposed reaction pathway network of GA by esterification, DODH and hydrogenation reactions. The reaction pathway network is based on our published paper [25].

+2, indicating that AC1 can stabilize a broad range of Re species (Table 4). We propose that other activated carbons (AC2 and AC3) behave alike. A similar trend is observed for ReO_x/CB, which also shows activity in the DODH reaction. In contrast, in the inactive ReO_x/GP catalyst, Re is found predominantly in its metallic form (67 %), which is consistent with previous reports indicating that metallic rhenium alone does not account for DODH activity [28,64,65,67]. Interestingly, the Re on MWCNT exhibits a broader distribution of oxidation states, with appreciable amounts of each rhenium oxidation state, and it is also the only one of the measured catalysts with Re(7+) present. As mentioned above, the limited catalytic activity of this material may be attributed to its relatively low amount of Re available on the surface. Nonetheless, XPS still detects underlying Re species, suggesting the presence of a subsurface Re-containing layer, although a detailed analysis of this layer lies beyond the scope of the present study.

In our previous work [27], we stated that the interactions between metallic Re and its high-valent oxo species are crucial for achieving high activity in the DODH reaction. We propose similar mechanism also for these catalysts. Although metallic form was not observed on XPS, due to reoxidation of Re to lower valent species for XPS transfer, it is an essential component of the active site, particularly for hydrogen activation. At the same time, the presence of high-valent Re oxo species cannot be excluded and is, in fact, expected. These high-valent species are widely recognised as crucial for the DODH step, while metallic Re facilitates hydrogenation reactions. The catalytic performance therefore most likely arises from a synergistic interplay between metallic and oxidic rhenium species, where the balance between different oxidation states is critical for achieving high activity and selectivity. To investigate whether only high-valent Re species alone are catalytically active and whether prior reduction is necessary, a control DODH reaction was performed using non-reduced ReO_x/AC1. The catalytic activity was significantly lower, reaching only a 46 % combined yield of methyl acrylate and acrylic acid after 72 h, compared to a 76 % combined yield under standard (pre-reduced) conditions (Fig. S8). XPS analysis of the non-reduced ReO_x/AC, before reaction, confirmed that Re was present in the +6-oxidation state (86 %) (Fig. S9 and Table S7). Based on these results, catalyst pre-treatment provides multiple oxidation state and is therefore beneficial for achieving higher DODH activity. Nevertheless, the redox behaviour of Re during the reaction is complex, and the precise catalytic cycle involving different oxidation states remains difficult to elucidate. This aspect should be explored in more detail in future studies to gain a deeper understanding of the reaction mechanism.

Unfortunately, although the ReO_x/AC1 catalyst exhibited excellent activity toward DODH, recycling tests (Fig. S10, Panel A) at 150 °C revealed a rapid loss of activity already after the second cycle, with the yield dropping below 10 %. However, this trend was observed for the commercial Re/C catalyst tested under identical conditions as well (Fig. S10, Panel B); it also showed a pronounced loss of performance after the first recycle, indicating that this deactivation is a general challenge for Re-based catalysts under DODH conditions [68]. The observed loss of catalytic activity may be partially attributed to rhenium leaching into the homogeneous phase, which was investigated by performing a hot filtration test on the Re/AC1 catalyst. As shown in Fig. S11, following catalyst removal the reaction proceeded mainly via esterification of acrylic acid to methyl acrylate, while only minor additional DODH activity was observed. Compared to the heterogeneous reaction, this contribution was negligible, indicating that the solid catalyst is responsible for the dominant DODH activity. These findings overall highlight the need to improve catalyst stability, for example through stronger metal–support interactions or structural modifications, to maintain activity and oxidation-state balance over multiple cycles.

4. Conclusion

This study investigated the influence of carbon-based supports on the catalytic performance of pre-reduced rhenium catalysts for the deoxydehydration (DODH) of glyceric acid in methanol. A series of Re-supported catalysts were prepared using seven structurally and chemically distinct carbon materials and tested at 150 °C under inert atmosphere for 72 h. Among the evaluated catalysts, activated carbon supports, ReO_x/AC1, ReO_x/AC2, and ReO_x/AC3, exhibited the highest selectivity toward the targeted DODH products—acrylic acid and methyl acrylate—with combined selectivities of 77 %, 83 %, and 59 %, respectively.

These results demonstrate that activated carbon supports (AC1, AC2, AC3) with high surface areas and mesoporous structures provide an efficient platform for enabling the formation of catalytically relevant rhenium species. In particular, the coexistence of high-valent Re species, which are essential for DODH, together with lower oxidation states required for hydrogen activation and hydrogenation, makes these catalysts highly effective for the conversion of glyceric acid to acrylic acid. In contrast, other supports such as CB, GC, GP, and MWCNT showed lower surface areas, less homogeneous Re distribution, and limited surface availability of Re species, correlating with their lower catalytic activity.

Importantly, this work demonstrates that Re catalysts can be effectively synthesized in-house, offering a cost-efficient alternative to commercial Re/C catalysts. The use of solid catalyst, as well as methanol as solvent and hydrogen donor for this process, present a great alternative for greener process, since both can be recovered and reused. Nevertheless, catalyst recyclability remains a major challenge, and improving the stability of supported Re species under reaction conditions is a critical avenue for future work.

CRediT authorship contribution statement

Maja Gabrič: Writing – original draft, Investigation, Data curation, Conceptualization. **Brigita Hočevar:** Writing – review & editing, Supervision. **Anej Blažič:** Methodology, Data curation. **Janvit Teržan:** Writing – review & editing, Supervision, Data curation. **Sašo Gyergyek:** Writing – original draft, Data curation. **Blaž Likozar:** Funding acquisition. **Miha Grilc:** Writing – review & editing, Supervision.

Declaration of competing interest

The authors declare that they have no known competing financial interests or personal relationships that could have appeared to influence the work reported in this paper.

Acknowledgements

This research was funded by the Slovenian Research and Innovation Agency (ARIS) through research projects; J1-3020, GC-0007, research program fundings; P2-0089 and P2-0152, and the access to research equipment via ARIS program P1-0417. Additional support was provided by the European Union's Horizon funding (Project 101070302). Lucija Kovaček and Urška Kavčič are acknowledged for their excellent experimental and moral support.

Appendix A. Supplementary data

Supplementary data to this article can be found online at https://doi.org/10.1016/j.carbon.2026.121244.

References

[1] R. Beerthuis, G. Rothenberg, N.R. Shiju, Catalytic routes towards acrylic acid, adipic acid and ε-caprolactam starting from biorenewables, Green Chem. 17 (2015) 1341–1361, https://doi.org/10.1039/C4GC02076F.
[2] J.L. Rodrigues, Heterologous production of acrylic acid: current challenges and perspectives, SynBio 1 (2022) 3–32, https://doi.org/10.3390/synbio1010002.

[3] H. Fouilloux, C.M. Thomas, Production and polymerization of biobased acrylates and analogs, Macromol. Rapid Commun. 42 (2021), https://doi.org/10.1002/marc.202000530.

[4] D. Sun, Y. Yamada, S. Sato, W. Ueda, Glycerol as a potential renewable raw material for acrylic acid production, Green Chem. 19 (2017) 3186–3213, https://doi.org/10.1039/C7GC00358G.

[5] A. Sandid, J. Esteban, C. D'Agostino, V. Spallina, Process assessment of renewable-based acrylic acid production from glycerol valorisation, J. Clean. Prod. 418 (2023) 138127, https://doi.org/10.1016/j.jclepro.2023.138127.

[6] U.C. Abubakar, Y. Bansod, L. Forster, V. Spallina, C. D'Agostino, Conversion of glycerol to acrylic acid: a review of strategies, recent developments and prospects, React. Chem. Eng. 8 (2023) 1819–1838, https://doi.org/10.1039/D3RE00057E.

[7] A. Abdullah, A.Z. Abdullah, M. Ahmed, P.U. Okoye, M. Shahadat, A review on bi/multifunctional catalytic oxydehydration of bioglycerol to acrylic acid: catalyst type, kinetics, and reaction mechanism, Can. J. Chem. Eng. 100 (2022) 2956–2985, https://doi.org/10.1002/cjce.24295.

[8] N.N. Tshibalonza, J.-C.M. Monbaliu, The deoxydehydration (DODH) reaction: a versatile technology for accessing olefins from bio-based polyols, Green Chem. 22 (2020) 4801–4848, https://doi.org/10.1039/D0GC00689K.

[9] A.R. Petersen, P. Fristrup, New motifs in deoxydehydration: beyond the realms of rhenium, Chem. Eur J. 23 (2017) 10235–10243, https://doi.org/10.1002/chem.201701153.

[10] F.C. Jentoft, Transition metal-catalyzed deoxydehydration: missing pieces of the puzzle, Catal. Sci. Technol. 12 (2022) 6308–6358, https://doi.org/10.1039/d1cy02083h.

[11] S. Raju, M.-E. Moret, R.J.M. Klein Gebbink, Rhenium-catalyzed dehydration and deoxydehydration of alcohols and polyols: opportunities for the formation of olefins from biomass, ACS Catal. 5 (2015) 281–300, https://doi.org/10.1021/cs501511x.

[12] J.S. Reinhold, J. Pang, B. Zhang, F.E. Kühn, T. Zhang, Rhenium-based catalysts for biomass conversion, Green Chem. 26 (2024) 10661–10686, https://doi.org/10.1039/D4GC02925A.

[13] M. Shiramizu, F.D. Toste, Deoxygenation of biomass-derived feedstocks: Oxorhenium-Catalyzed deoxydehydration of sugars and sugar alcohols, Angew. Chem. Int. Ed. 51 (2012) 8082–8086, https://doi.org/10.1002/anie.201203877.

[14] R.T. Larson, A. Samant, J. Chen, W. Lee, M.A. Bohn, D.M. Ohlmann, S.J. Zuend, F. D. Toste, Hydrogen gas-mediated deoxydehydration/hydrogenation of sugar acids: catalytic conversion of glucarates to adipates, J. Am. Chem. Soc. 139 (2017) 14001–14004, https://doi.org/10.1021/jacs.7b07801.

[15] D.S. Morris, K. van Rees, M. Curcio, M. Cokoja, F.E. Kühn, F. Duarte, J.B. Love, Deoxydehydration of vicinal diols and polyols catalyzed by pyridinium perrhenate salts, Catal. Sci. Technol. 7 (2017) 5644–5649, https://doi.org/10.1039/C7CY01728F.

[16] Y. Stöckl, F. Rominger, A.S.K. Hashmi, T. Schaub, Insights for the hydrogen-mediated deoxydehydration (DODH) with Cp*ReO $_3$ and alkene extrusion of related Re(V)-Diolates, ChemCatChem 17 (2025) e202402010, https://doi.org/10.1002/cctc.202402010.

[17] L. Sandbrink, E. Klindtworth, H.U. Islam, A.M. Beale, R. Palkovits, ReOx/TiO2: a recyclable solid catalyst for deoxydehydration, ACS Catal. 6 (2016) 677–680, https://doi.org/10.1021/acscatal.5b01936.

[18] B.E. Sharkey, F.C. Jentoft, Fundamental insights into deactivation by leaching during rhenium-catalyzed deoxydehydration, ACS Catal. 9 (2019) 11317–11328, https://doi.org/10.1021/acscatal.9b02806.

[19] B.E. Sharkey, A.L. Denning, F.C. Jentoft, R. Gangadhara, T. V Gopaladasu, K. M. Nicholas, New solid oxo-rhenium and oxo-molybdenum catalysts for the deoxydehydration of glycols to olefins, Catal. Today 310 (2018) 86–93, https://doi.org/10.1016/j.cattod.2017.05.090.

[20] Y. Nakagawa, S. Tazawa, T. Wang, M. Tamura, N. Hiyoshi, K. Okumura, K. Tomishige, Mechanistic Study of Hydrogen-Driven Deoxydehydration over Ceria-Supported Rhenium Catalyst Promoted by Au Nanoparticles, ACS Catal. 8 (2018) 584–595, https://doi.org/10.1021/acscatal.7b02879.

[21] K. Yamaguchi, J. Cao, M. Betchaku, Y. Nakagawa, M. Tamura, A. Nakayama, M. Yabushita, K. Tomishige, Deoxydehydration of biomass-derived polyols over silver-modified ceria-supported rhenium catalyst with molecular hydrogen, ChemSusChem 15 (2022) e202102663, https://doi.org/10.1002/cssc.202102663.

[22] T. Wang, S. Liu, M. Tamura, Y. Nakagawa, N. Hiyoshi, K. Tomishige, One-pot catalytic selective synthesis of 1,4-butanediol from 1,4-anhydroerythritol and hydrogen, Green Chem. 20 (2018) 2547–2557, https://doi.org/10.1039/C8GC00574E.

[23] M. Tamura, N. Yuasa, J. Cao, Y. Nakagawa, K. Tomishige, Transformation of sugars into chiral polyols over a heterogeneous catalyst, Angew. Chem. Int. Ed. 57 (2018) 8058–8062, https://doi.org/10.1002/anie.201803043.

[24] S. Larasati, Y. Nakagawa, M. Yabushita, K. Tomishige, Reusable ReO $_x$ -Pd/CeO $_2$ catalyst with low metal surface concentration for efficient consecutive deoxydehydration and hydrogenation of vicinal OH groups, Adv. Energy Sustain. Res. 6 (2025) 2400363, https://doi.org/10.1002/aesr.202400363.

[25] M. Gabrič, F.M. Harth, B. Hočevar, S. Gyergyek, B. Likozar, M. Grilc, A H2-free heterogeneous route to glycerol-based acrylics via Re-based deoxydehydration, Green Chem. 27 (2025) 3640–3645, https://doi.org/10.1039/D5GC00445D.

[26] B. Hočevar, A. Prašnikar, S. Gyergyek, M. Huš, M. Grilc, B. Likozar, Multiscale kinetic modelling of de-hydroxylation of mucic- to adipic acid esters over Re/C, J. Ind. Eng. Chem. 147 (2025) 668–682, https://doi.org/10.1016/j.jiec.2024.12.058.

[27] F.M. Harth, M. Gabrič, J. Teržan, B. Hočevar, S. Gyergyek, B. Likozar, M. Grilc, Tailoring selective de-hydroxylation/hydrogenation reactions of bio-based aldaric acids towards adipic acid derivatives by re catalyst metal–support interactions, Catal. Today 441 (2024) 114879, https://doi.org/10.1016/j.cattod.2024.114879.

[28] D.K. Mishra, C.C. Truong, Y. Jo, Y.-W. Suh, Recent catalytic advances in the production of adipic acid and its esters from bio-based C6 molecules and carbon dioxide, Green Chem. Lett. Rev. 18 (2025) 2457497, https://doi.org/10.1080/17518253.2025.2457497.

[29] J.H. Jang, I. Ro, P. Christopher, M.M. Abu-Omar, A heterogeneous Pt-ReOx/C catalyst for making renewable adipates in one step from sugar acids, ACS Catal. 11 (2021) 95–109, https://doi.org/10.1021/acscatal.0c04158.

[30] B. Hočevar, A. Prašnikar, M. Huš, M. Grilc, B. Likozar, H2-Free Re-Based catalytic dehydroxylation of aldaric acid to muconic and adipic acid esters, Angew. Chem., Int. Ed. 60 (2021) 1244–1253, https://doi.org/10.1002/anie.202010035.

[31] E. Lam, J.H.T. Luong, Carbon materials as catalyst supports and catalysts in the transformation of biomass to fuels and chemicals, ACS Catal. 4 (2014) 3393–3410, https://doi.org/10.1021/cs5008393.

[32] P. Serp, J.L. Figueiredo, Carbon Materials for Catalysis, John Wiley & Sons, New Jersey, 2009.

[33] A. Bahuguna, A. Kumar, V. Krishnan, Carbon-support-based heterogeneous nanocatalysts: synthesis and applications in organic reactions, Asian J. Org. Chem. 8 (2019) 1263–1305, https://doi.org/10.1002/ajoc.201900259.

[34] D.S. Su, S. Perathoner, G. Centi, Nanocarbons for the development of advanced catalysts, Chem. Rev. 113 (2013) 5782–5816, https://doi.org/10.1021/cr300367d.

[35] H.C. Kwon, S. Yook, S. Choi, M. Choi, Comprehensive understanding of the effects of carbon nanostructures on redox catalytic properties and stability in oxidative dehydrogenation, ACS Catal. 7 (2017) 5257–5267, https://doi.org/10.1021/acscatal.7b01742.

[36] F. Rodríguez-reinoso, The role of carbon materials in heterogeneous catalysis, Carbon N Y 36 (1998) 159–175, https://doi.org/10.1016/S0008-6223(97)00173-5.

[37] X. Fan, G. Zhang, F. Zhang, Multiple roles of graphene in heterogeneous catalysis, Chem. Soc. Rev. 44 (2015) 3023–3035, https://doi.org/10.1039/C5CS00094G.

[38] M.B. Burkholder, F.B.A. Rahman, E.H. Chandler, J.R. Regalbuto, B.F. Gupton, J.M. M. Tengco, Metal supported graphene catalysis: a review on the benefits of nanoparticular supported specialty sp2 carbon catalysts on enhancing the activities of multiple chemical transformations, Carbon Trends 9 (2022) 100196, https://doi.org/10.1016/j.cartre.2022.100196.

[39] Y. Zheng, L. Lin, B. Wang, X. Wang, Graphitic carbon nitride polymers toward sustainable photoredox catalysis, Angew. Chem. Int. Ed. 54 (2015) 12868–12884, https://doi.org/10.1002/anie.201501788.

[40] A.D. Dobrzańska-Danikiewicz, W. Wolany, G. Benke, Z. Rdzawski, The new MWCNTs-rhenium nanocomposite, Phys. Status Solidi B Basic Res. 251 (2014) 2485–2490, https://doi.org/10.1002/pssb.201451360.

[41] A.D. Dobrzańska-Danikiewic, W. Wolany, D. Cichocki, D. Łukowiec, Microscopic and spectroscopic research of the MWCNTs-Re nanocomposites, Arch. Metall. Mater. 60 (2015) 2047–2051, https://doi.org/10.1515/amm-2015-0347.

[42] M. Melchionna, S. Marchesan, M. Prato, P. Fornasiero, Carbon nanotubes and catalysis: the many facets of a successful marriage, Catal. Sci. Technol. 5 (2015) 3859–3875, https://doi.org/10.1039/C5CY00651A.

[43] M. Jin, M. Choi, Hydrothermal deoxygenation of triglycerides over carbon-supported bimetallic PtRe catalysts without an external hydrogen source, Mol. Catal. 474 (2019) 110419, https://doi.org/10.1016/j.mcat.2019.110419.

[44] D.S. Park, O.A. Abdelrahman, K.P. Vinter, P.M. Howe, J.Q. Bond, T.M. Reineke, K. Zhang, P.J. Dauenhauer, Multifunctional Cascade catalysis of itaconic acid hydrodeoxygenation to 3-Methyl-tetrahydrofuran, ACS Sustain. Chem. Eng. 6 (2018) 9394–9402, https://doi.org/10.1021/acssuschemeng.8b01743.

[45] P.U. Karanjkar, S.P. Burt, X. Chen, K.J. Barnett, M.R. Ball, M.D. Kumbhalkar, X. Wang, J.B. Miller, I. Hermans, J.A. Dumesic, G.W. Huber, Effect of carbon supports on RhRe bifunctional catalysts for selective hydrogenolysis of tetrahydropyran-2-methanol, Catal. Sci. Technol. 6 (2016) 7841–7851, https://doi.org/10.1039/c6cy01763k.

[46] V. Calvino-Casilda, A.J. Lopez-Peinado, C.J. Duran-Valle, R.M. Martin-Aranda, Last decade of research on activated carbons as catalytic support in chemical processes, Catal. Rev. Sci. Eng. 52 (2010) 325–380, https://doi.org/10.1080/01614940.2010.498748.

[47] M. Iwanow, T. Gärtner, V. Sieber, B. König, Activated carbon as catalyst support: precursors, preparation, modification and characterization, Beilstein J. Org. Chem. 16 (2020) 1188–1202, https://doi.org/10.3762/bjoc.16.104.

[48] E. Blanco, P. Cabeza, V. Naharro Ovejero, C. Contreras, A.B. Dongil, I. T. Ghampson, N. Escalona, Effect of carbon support and functionalization on the synthesis of rhenium carbide and its use on HDO of guaiacol, Catal. Today 420 (2023) 114031, https://doi.org/10.1016/j.cattod.2023.02.008.

[49] E. Blanco, A.B. Dongil, I.T. Ghampson, N. Escalona, Effect of the support on rhenium carbide in the hydrodeoxygenation of guaiacol as lignin-derived model compound, Catalysts 12 (2022) 1229, https://doi.org/10.3390/catal12101229.

[50] E. Blanco, A.B. Dongil, J.L. García-Fierro, N. Escalona, Insights in supported rhenium carbide catalysts for hydroconversion of lignin-derived compounds, Appl. Catal. Gen. 599 (2020) 117600, https://doi.org/10.1016/j.apcata.2020.117600.

[51] E. Blanco, C. Sepulveda, K. Cruces, J.L. García-Fierro, I.T. Ghampson, N. Escalona, Conversion of guaiacol over metal carbides supported on activated carbon catalysts, Catal. Today 356 (2020) 376–383, https://doi.org/10.1016/j.cattod.2019.08.029.

[52] R.P. Rocha, M.F.R. Pereira, J.L. Figueiredo, Characterisation of the surface chemistry of carbon materials by temperature-programmed desorption: an assessment, Catal. Today 418 (2023) 114136, https://doi.org/10.1016/j.cattod.2023.114136.

[53] M. Iwanow, T. Gärtner, V. Sieber, B. König, Activated carbon as catalyst support: precursors, preparation, modification and characterization, Beilstein J. Org. Chem. 16 (2020) 1188–1202, https://doi.org/10.3762/bjoc.16.104.
[54] J.L. Figueiredo, M.F.R. Pereira, The role of surface chemistry in catalysis with carbons, Catal. Today 150 (2010) 2–7, https://doi.org/10.1016/j.cattod.2009.04.010.
[55] Y.T. Kim, J.A. Dumesic, G.W. Huber, Aqueous-phase hydrodeoxygenation of sorbitol: a comparative study of Pt/Zr phosphate and PtReOx/C, J. Catal. 304 (2013) 72–85, https://doi.org/10.1016/j.jcat.2013.03.022.
[56] S.T. Thompson, H.H. Lamb, Vapor-phase hydrodeoxygenation of guaiacol over carbon-supported Pd, re and PdRe catalysts, Appl. Catal. Gen. 563 (2018) 105–117, https://doi.org/10.1016/j.apcata.2018.06.031.
[57] X. Di, C. Li, G. Lafaye, C. Especel, F. Epron, C. Liang, Influence of Re-M interactions in Re-M/C bimetallic catalysts prepared by a microwave-assisted thermolytic method on aqueous-phase hydrogenation of succinic acid, Catal. Sci. Technol. 7 (2017) 5212–5223, https://doi.org/10.1039/c7cy01039g.
[58] J. Ullrich, B. Breit, Selective hydrogenation of carboxylic acids to alcohols or alkanes employing a heterogeneous catalyst, ACS Catal. 8 (2018) 785–789, https://doi.org/10.1021/acscatal.7b03484.
[59] F.M. Harth, M. Grilc, B. Likozar, Liquid-phase process for the production of acrylic acid esters from glyceric acid, PCT/EP2023/070258 (2023).
[60] A.L. Denning, H. Dang, Z. Liu, K.M. Nicholas, F.C. Jentoft, Deoxydehydration of glycols catalyzed by carbon-supported perrhenate, ChemCatChem 5 (2013) 3567–3570, https://doi.org/10.1002/cctc.201300545.
[61] E. Ochoa, D. Torres, J.L. Pinilla, I. Suelves, Nanostructured carbon material effect on the synthesis of carbon-supported molybdenum carbide catalysts for guaiacol hydrodeoxygenation, Energies 13 (2020) 1189, https://doi.org/10.3390/en13051189.
[62] A.B. Dongil, E. Blanco, J.J. Villora-Picó, A. Sepúlveda-Escribano, I. Rodríguez-Ramos, Effect of the carbon support and conditions on the carbothermal synthesis of Cu-Molybdenum carbide and its application on CO2 hydrogenation to methanol, Nanomaterials 12 (2022) 1048, https://doi.org/10.3390/nano12071048.
[63] R. Ganjoo, S. Sharma, A. Kumar, M.M.A. Daouda, Activated carbon: fundamentals, classification, and properties, in: Activated Carbon, The Royal Society of Chemistry, 2023, pp. 1–22, https://doi.org/10.1039/BK9781839169861-00001.
[64] K.S.W. Sing, Reporting physisorption data for gas/solid systems with special reference to the determination of surface area and porosity (recommendations 1984), Pure Appl. Chem. 57 (1985) 603–619, https://doi.org/10.1351/pac198557040603.
[65] K. Moyer-Vanderburgh, S.J. Park, F. Fornasiero, Growth of carbon nanotube forests on flexible metal substrates: advances, challenges, and applications, Carbon N Y 206 (2023) 402–421, https://doi.org/10.1016/j.carbon.2023.02.054.
[66] T. Wang, Y. Nakagawa, M. Tamura, K. Okumura, K. Tomishige, Tungsten–zirconia-supported rhenium catalyst combined with a deoxydehydration catalyst for the one-pot synthesis of 1,4-butanediol from 1,4-anhydroerythritol, React. Chem. Eng. 5 (2020) 1237–1250, https://doi.org/10.1039/D0RE00085J.
[67] M.T. Greiner, T.C.R. Rocha, B. Johnson, A. Klyushin, A. Knop-Gericke, R. Schlögl, The oxidation of rhenium and identification of rhenium oxides during catalytic partial oxidation of ethylene: an In-Situ XPS study, Z. Phys. Chem. 228 (2014) 521–541, https://doi.org/10.1515/zpch-2014-0002.
[68] F.M. Harth, B. Likozar, M. Grilc, Stability of solid rhenium catalysts for liquid-phase biomass valorization–various facets of catalyst deactivation and rhenium leaching, Mater. Today Chem. 26 (2022) 101191, https://doi.org/10.1016/j.mtchem.2022.101191.